Axial Attitude Estimation of Spacecraft in Orbit Based on ISAR Image Sequence

Peng Kou ⬤, Yongxiang Liu ⬤, Weijun Zhong, Biao Tian ⬤, WenZhen Wu, and Chi Zhang ⬤

Abstract—**Attitude estimation is a significant task for monitoring noncooperative spacecraft in orbit. Inverse synthetic aperture radar (ISAR) is an effective method to obtain the structure, size, and attitude of spacecraft. Most existing methods of attitude estimation based on ISAR images generally rely on characteristic point matching or rectangular feature matching among ISAR images. They often need high quality ISAR images, so the robustness is usually poor. A novel method for estimating spacecraft's axial attitude in ISAR image is proposed in this article. This method does not need to utilize a simulation database, or to match sequence of specific features, so it has good robustness. Our method bridges Range–Doppler images and attitude parameters with the accommodation of spacecraft's orbit parameters and the ISAR geometric projection model. Based on the ISAR imaging turntable model, the accurate position of the imaging plane of the spacecraft in orbit is derived. Then, attitude parameters are estimated by an optimization of the projection of spacecraft's three-dimensional model to the imaging plane. Experimental results demonstrate the effectiveness and robustness of the proposed method to estimate attitude of spacecraft in orbit by the simulated and measured ISAR images.**

Index Terms—**Axial attitude estimation, inverse synthetic aperture radar (ISAR) image sequence, imaging plane, rolling spacecraft.**

I. INTRODUCTION

THE attitude of spacecraft in orbit can be roughly divided into stable attitude or rolling attitude. For most rigid spacecraft, the attitude of spacecraft in orbit can be expressed by axial attitude, such as Main axis, Solar panel axis, etc. It is the main characteristic to describe the motion of spacecraft in orbit and is important for rescuing faults, obtaining action intention, and predicting re-entry [1].

The spacecraft's attitude is generally described by three angles, i.e., the yaw, pitch and roll in the orbit coordinate system.

Peng Kou is with the College of Electronic Science, National University of Defense Technology, Changsha 410073, China and also with the Xi'an Satellite Control Center, Xi'an 710000, China (e-mail: kou_810518@163.com).

Yongxiang Liu, Biao Tian, WenZhen Wu, and Chi Zhang are with the College of Electronic Science, National University of Defense Technology, Changsha 410073, China (e-mail: lyx_bible@sina.com; tbncsz@126.com; 18768117728@163.com; zcnudt@126.com).

Weijun Zhong is with the Xi'an Satellite Control Center, Xi'an 710600, China (e-mail: 125525956@qq.com).

For cooperative spacecraft, attitude parameters in orbit is obtained through various attitude sensor measurements in spacecraft [2]. For noncooperative spacecraft, the precise attitude in orbit cannot be obtained due to the invalid of the telemetry signal [3]. Thus, adaptive optics imaging telescope or inverse synthetic aperture radar (ISAR) are often used to estimate the attitude of noncooperative spacecraft. The adaptive optical image has the characteristics of intuitive imaging and a clear image plane position. However, due to the influence of sunlight, earth shadow, atmospheric turbulence, and weather, the timeliness and quality of adaptive optical image are difficult to be guaranteed in practical application. By contrast, ISAR has the advantages of all-weather and all-time observation capability, so it has become an important way to estimate the attitude of spacecraft. Suwa *et al.* [4] achieved promising results by using multistatic ISAR to estimate the spacecraft attitude. But at present, there are still difficulties in ISAR imaging of spacecraft with multibase radar in practical engineering. It is ill-conditioned to estimate the three-dimensional (3-D) attitude angle from a single ISAR image. Therefore, the ISAR sequence is needed to realize the inversion from 2-D imaging plane to 3-D attitude.

The ISAR image in orbit can be regarded as the projection of the 3-D structure of the spacecraft on the imaging plane [5]. Therefore, determining the ISAR imaging plane is the essential step for attitude estimation. Different from optical imaging, the imaging plane of ISAR image is closely related to radar line of sight (LOS) and the motion of spacecraft. Chen *et al.* [6] analyzed the ISAR imaging plane in inertial and three-axis attitude stabilization. However, for the spacecraft in rolling attitude, the position of the equivalent imaging plane will be changed in the coherent processing interval (CPI). Therefore, this article first analyzes the position of equivalent imaging plane with various attitudes.

Reviewing relevant studies, there are two kinds of methods to estimate the attitude of spacecraft. One is to estimate the structure, size, and attitude of spacecraft by 3-D reconstruction [7], [8]. The core of this method is to obtain the projection matrix of the scattering points in different attitudes [9], [10]. Unfortunately, the phenomenon like "angular glint," "cavity scattering" may also occur in high-frequency radar measurements. So the position of some scattering points may be changed with LOS. These phenomenon will make feature association among ISAR images even more difficult [11]. The second one is the template matching, which usually needs to acquire appropriate features [12], [13]. These features mainly include radar cross section, HRRP, and ISAR imagery. But this method requires

the prior information of structure, size, and so on. Moreover, it may be sensitive to noise and can not be used when the LOS changes dramatically. Recently, a method was proposed by Zhou *et al.* [14] based on rectangular feature matching. When some ISAR sequence images of spacecraft have rectangular structure, this method performs well. But it may be difficult to extract rectangular features from some measured ISAR images of spacecraft, which is shown in Experiment Part B. Moreover, the accuracy of attitude estimation depends on the performance of ISAR imaging algorithm. This requires higher image quality and resolution.

For attitude rolling spacecraft, Rosebrick [3] proposed a method to estimate the cross-range scale and spacecraft attitude of ISAR images by stereo vision algorithm. This method needs to know the following parameters: 1) attitude of the spacecraft at an initial time instance; 2) rotational velocity vector at the initial time instance; 3) Main axis of inertia and moments of inertia. These conditions are usually difficult to know in practical application. Zhou *et al.* [15] used multiple-station ISAR images method to estimate the rolling parameters. However, this method requires multiple radars to observe the same target accurately and synchronously.

In this article, we propose a method for estimating axial attitude of spacecraft in orbit. According to the ISAR imaging projection theory, the ISAR imaging procedure of spacecraft is to project 3-D scattering points on a 2-D radar imaging plane. First, our method deduces the position of ISAR imaging plane. Then, the 2-D direction of axial attitude is extracted by using the continuous changes in the ISAR image sequence. Subsequently, the actual 3-D attitude of the spacecraft is solved by using the relationship of imaging projection. Compared with most existing attitude estimation methods, this method has some innovations as follows.

1) In the existing literature, ISAR imaging plane analysis is mostly for attitude stabilized spacecraft in orbit. The analytical expression of ISAR imaging plane for attitude rolling spacecraft has not been found as we know. In this article, based on the rigid body 3-D rotation model, the mathematical expression of ISAR imaging plane for attitude rolling spacecraft is derived. At the same time, we also analyze how to choose the best equivalent imaging time in CPI, which means the time corresponding to the formation of the imaging plane.

2) Compared with traditional line detection methods such as Hough transform and Radon transform, we proposed a method based on morphological linear structure erosion for direction estimation of axis in ISAR image. It detects the direction of dense scattering points instead of rectangular structure or feature point, so this method is not sensitive to noise. Even under adverse conditions, such as "angular glint," "cavity scattering," and certain "defocusing" could not affect the estimation results in ISAR image. All in all, it is more robustness than the existing methods based on rectangular structure or feature point.

3) To the best of our knowledge, it is the first time to establish a unified motion model of spacecraft with attitude stability and rolling for a single radar station. Different from the
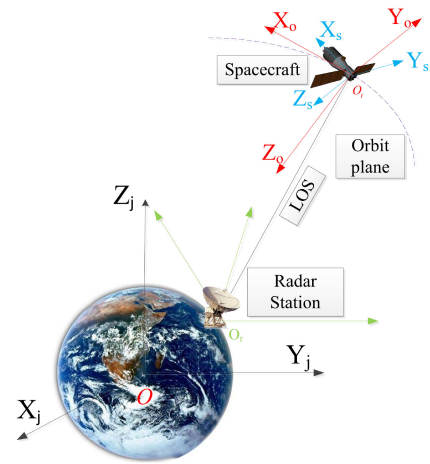

Fig. 1. Definitions of related coordinate systems.

conventional methods, it can be executed independently to estimate axial attitude without obtaining its structure knowledge in advance. The re-entry of Tiangong-1 is used based on the simulated and measured data to verify the accuracy and practicability of our method.

What we need to emphasize is that the proposed method relies on the results of cross-range scaled for ISAR images. Base on [16]– [18], an equivalent rotation angular velocity model and other methods are used to estimate the rotation angle, to realize the cross-range scaling of noncooperative spacecraft. It is ensured the adaptability of our proposed methods.

This article is organized as follows. In Section II, several coordinate systems are introduced and the parameters of spacecraft's attitude in orbit are given. In Section III, motion model of attitude rolling spacecraft is established and ISAR imaging plane is derived. In Section IV, the ISAR image axial extraction is realized by morphological linear erosion method, and the spacecraft attitude and rolling motion parameters are retrieved, then the algorithm flow chart is given. In Section V, experimental results based on simulated and measured data are presented to show the effectiveness and robustness of the proposed method. Finally, Section VI concludes this article.

II. DEFINITION OF COORDINATE SYSTEMS AND THE PARAMETERS OF SPACECRAFT'S ATTITUDE IN ORBIT

In this section, several coordinate systems are introduced, then the parameters of spacecraft's attitude in orbit are given.

A. Definition and Relationship of Related Coordinate Systems

As shown in Fig. 1, three coordinate origins are defined as follows: the earth's centroid is O, the spacecraft's centroid is O_t, the radar's centroid is O_r.

1) J2000.0 inertial coordinate system $O - X_j Y_j Z_j$.

2) Orbit coordinate system $O_t - X_o Y_o Z_o$.

The detailed definitions of (1) and (2) coordinate systems are given in Appendix A. The transformation matrix from J2000.0 coordinate system to orbit coordinate system is C_{j2o}, which is also described in Appendix A.
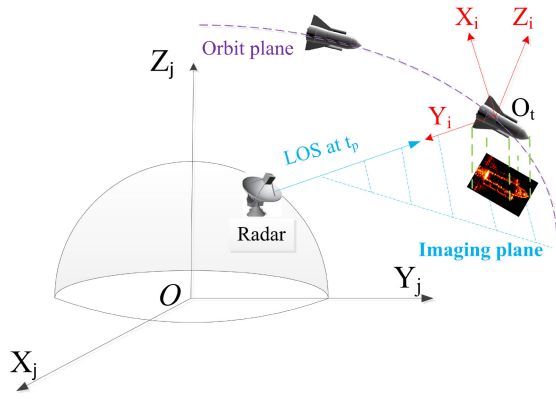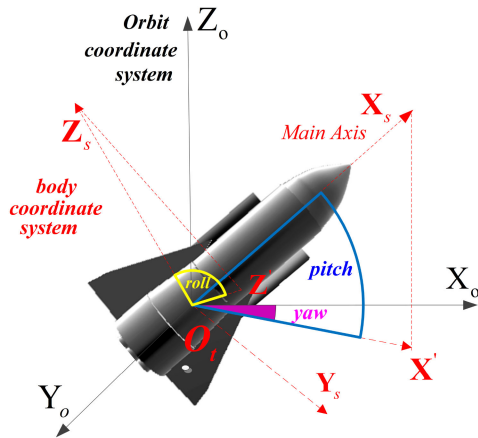
Fig. 2.   Imaging coordinate system.

Fig. 3.   Definition of spacecraft's attitude in orbit.

3) Body coordinate system $O_t - X_s Y_s Z_s$.

As shown in Fig. 1, the coordinate origin is O_t, the axis X_s points to the direction of the Main axis (the longest axis) of the spacecraft, the axis Y_s points to inertia axis (the second longest axis), and the axis X_s, Y_s, Z_s forms a right-hand system. For the attitude stabilization spacecraft, the angle between the body coordinate system and the orbit coordinate system is fixed or coincided.

4) Roll coordinate system $O_t - X_p Y_p Z_p$.

The coordinate origin is O_t, take the roll axis as the axis Z_p. At the initial moment, the axis Y_p is on the plane determined by Z_p and the Main axis. The axis X_p forms a right-hand system with Y_p and Z_p. The details are given in Section III-B.

5) Imaging coordinate system $O_t - X_i Y_i Z_i$.

As shown in Fig. 2, the coordinate origin is O_t, the radar's LOS negative direction at t_p is taken as the axis Y_i, and the equivalent rotation axis is defined as the Z_i axis. The derivation of Z_i is shown in Section III-B. The axis X_i forms a right-hand system with Y_i and Z_i. Usually, t_p is selected in the middle time of CPI, which is described in Appendix B.

B. Parameters of Spacecraft's Attitude in Orbit

As shown in Fig. 3, $O_t X_s$ is the Main axis of spacecraft. The attitude angle of spacecraft is defined as the relationship between

Angle	*Yaw*	*Pitch*	*Roll*
Meaning	$\angle X_o O_t X'$	$\angle X_s O_t X'$	$\angle Z_o O_t Z'$

Orbit coordinate system $O_t - X_o Y_o Z_o$ and Ontological coordinate system $O_t - X_s Y_s Z_s$, which can be described by yaw, pitch and roll. See Table I for detailed parameter meaning. $O_t X'$ is the vector projected from $O_t X_s$ to $X_o O_t Y_o$ plane, $O_t Z'$ is the vector projected from $O_t Z_s$ to $X_o O_t Y_o$ plane.

Rolling motion could be regarded as rotating around a certain rotation shaft with a certain rotation speed [15]. For the rolling spacecraft, since the attitude angle may be changed with time, attitude estimation can be used to estimate rotation shaft and rotation speed instead. The details are given in Section III-B.

III. MOTION MODEL OF ATTITUDE ROLLING SPACECRAFT AND ANALYSIS OF ISAR IMAGING PLANE

An observable segment time (AOST) duration the ground-based ISAR imaging radar to low earth orbit spacecraft is usually no more than twenty minutes [14]. For the attitude stable spacecraft, the attitude angle is considered to be invariant in the orbit coordinate system. According to relevant researches of ENVISAT [19]–[21], the spin period of spacecraft is almost at the 160-s magnitude. From the research on Tiangong-1 [22], it is found that the rotation shaft and rotation speed are stable in the AOST in the inertial system. Therefore, in this article, the rotation shaft and rotation speed are assumed to be constant in AOST.

A. Analysis of ISAR Imaging Plane

In the case of spacecraft without micromotion parts, imaging plane in orbit can be deduced from the knowledge of rigid body mechanics. According to ISAR imaging turntable model and Range– Doppler (RD) imaging algorithm [23], at the moment of t, the LOS vector $\mathbf{L}(t)$ from radar to spacecraft centroid is range direction. The direction of equivalent rotation angle vector $\overrightarrow{\Omega}_{eff}$ is cross-range direction. The cross product of $\mathbf{L}(t)$ and $\overrightarrow{\Omega}_{eff}$ is the equivalent rotation axis, i.e., the normal vector of imaging plane. In J2000.0 inertial coordinate system, the position vector of spacecraft is $\mathbf{P}(t)$, the position vector of radar is $\mathbf{R}(t)$, and the LOS direction vector of centroid of radar and spacecraft is

$$\mathbf{L}(t) = \mathbf{P}(t) - \mathbf{R}(t). \qquad (1)$$

As shown in the Fig. 4, the relative rotation angular velocity $\overrightarrow{\Omega}_{LOS}$ of LOS is

$$\overrightarrow{\Omega}_{LOS} = \frac{\mathbf{L}(t)}{\|\mathbf{L}(t)\|^2} \times \frac{d\mathbf{L}(t)}{dt}. \qquad (2)$$

Set the position of any point in the spacecraft body coordinate system as $\mathbf{r}_0 = [x_0, y_0, z_0]^T$, $\mathbf{r}_0$ rotates at an angular velocity
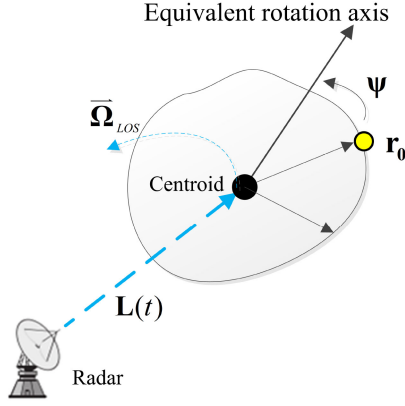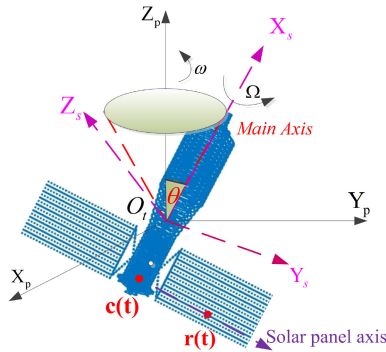
Fig. 4. ISAR imaging model of rigid body.

Fig. 5. Motion model of rolling spacecraft.

$\psi = [\psi_x, \psi_y, \psi_z]^T$ around its centroid, the equivalent observation angular velocity $\overrightarrow{\Omega}_{eff}$ of the radar to the point is

$$\overrightarrow{\Omega}_{eff} = \overrightarrow{\Omega}_{LOS} - \psi. \tag{3}$$

The key to the determination of imaging plane is to calculate ψ. For the three-axis attitude stabilized spacecraft with geocentric orientation [6], it can be solved by

$$\psi = \frac{\mathbf{P}(t)}{\|\mathbf{P}(t)\|^2} \times \frac{d\mathbf{P}(t)}{dt}. \tag{4}$$

B. Motion Model of Rolling Spacecraft and the Deduction of Imaging Plane

The roll motion can be divided into two motion components: the spin around the spacecraft body to the symmetric axis $O_t X_s$ and the conic rotation around the cone axis rotation shaft $O_t Z_p$. As shown in the Fig. 5, the angle between $O_t X_s$ and $O_t Z_p$ is θ, which is defined as rotation angle. The spacecraft cone rotation speed is ω, spin rotation speed is Ω. We define the three Euler angles of the transformation from rolling coordinate system to J2000.0 inertial coordinate system as α_{p2j}, β_{p2j}, γ_{p2j}. Axis attitude estimation can be used to estimate θ, ω, Ω, α_{p2j}, β_{p2j}, and γ_{p2j} equivalently.

The coordinate transformation from the body coordinate system to the roll coordinate system consists of three parts: the initial transformation matrix $\mathbf{R_{init}}$, the spin transformation matrix $\mathbf{R_{spin}}$, and the conic rotation transformation matrix $\mathbf{R_{coni}}$

[24]. They can be express as follows:

$$\mathbf{R}_{\text{coni}}(t) = \exp\left[\mathbf{e}_{\text{coni}} \cdot (\omega t)\right] \tag{5}$$

$$\mathbf{R}_{\text{init}} = \exp\left[\mathbf{e}_{\text{init}} \cdot \theta\right] \tag{6}$$

$$\mathbf{R}_{\text{spin}}(t) = \exp\left[\mathbf{e}_{\text{spin}} \cdot (\Omega t)\right] \tag{7}$$

where $\mathbf{e}_{\text{coni}} = \begin{bmatrix} 0 & -1 & 0 \\ 1 & 0 & 0 \\ 0 & 0 & 0 \end{bmatrix}$, $\mathbf{e}_{\text{init}} = \begin{bmatrix} 0 & 0 & 0 \\ 0 & 0 & -1 \\ 0 & 1 & 0 \end{bmatrix}$

$\mathbf{e}_{\text{spin}} = \begin{bmatrix} 0 & -1 & 0 \\ 1 & 0 & 0 \\ 0 & 0 & 0 \end{bmatrix}$.

Supposing $\mathbf{R}^r(t) = \mathbf{R}_{\text{coni}}(t) \cdot \mathbf{R}_{\text{init}} \cdot \mathbf{R}_{\text{spin}}(t)$, $\mathbf{R}^r(t)$ is a 3 row and 3 column matrix, $\mathrm{R}_{i,j}^r(i, j = 1, 2, 3)$ representing the elements in the ith row and jth column. At the time t, the position of $\mathbf{r}_0$ in the Roll coordinate system can be expressed as $\mathbf{r}(t)$

$$\mathbf{r}(t) = \mathbf{R}^r(t) \cdot \mathbf{r}_0. \tag{8}$$

According to the relationship between linear velocity and angular velocity, ψ can be obtained from the following equation:

$$\psi = \frac{\mathbf{r}(t) \times \dot{\mathbf{r}}(t)}{\|\mathbf{r}(t)\|} = \frac{\mathbf{r}(t) \times \dot{\mathbf{r}}(t)}{\|\mathbf{r}_0\|} \tag{9}$$

$\dot{\mathbf{r}}(t)$ means $\frac{d\mathbf{r}(t)}{dt}$, it can be expressed as

$$\dot{\mathbf{r}}(t) = [\omega \mathbf{e}_{\text{coni}} \mathbf{R}_{\text{coni}}(t) \mathbf{R}_{\text{init}} \mathbf{R}_{\text{spin}}(t) + \dot{\theta} \mathbf{R}_{\text{coni}}(t) \mathbf{e}_{\text{init}} \mathbf{R}_{init} \mathbf{R}_{\text{spin}}(t)$$
$$+ \Omega \mathbf{R}_{\text{coni}}(t) \mathbf{R}_{\text{init}} \mathbf{e}_{\text{spin}} \mathbf{R}_{\text{spin}}(t)] \mathbf{r}_0 \tag{10}$$

$\dot{\theta}$ means $\frac{d\theta}{dt}$, due to θ is a constant variable, so $\dot{\theta} = 0$. We define $\mathbf{M}$ as below

$$\mathbf{M}(t) = \omega \mathbf{e}_{\text{coni}} \mathbf{R}^r(t) + \Omega \mathbf{R}_{\text{coni}}(t) \mathbf{R}_{\text{init}} \mathbf{e}_{\text{spin}} \mathbf{R}_{\text{spin}}(t). \tag{11}$$

Equation (10) can be simplified as follow:

$$\dot{\mathbf{r}}(t) = \mathbf{M}(t) \cdot \mathbf{r}_0. \tag{12}$$

It is known that the derivative of a variable is itself multiplied by a coefficient. For the rotation matrix in 3-D space, there is the following expression:

$$\dot{\mathbf{r}}(t) = \overset{\wedge}{\psi} \cdot \mathbf{R}^r(t) \cdot \mathbf{r}_0 \tag{13}$$

where $\psi^\wedge$ is antisymmetric matrices with diagonal zero, it can be express as

$$\overset{\wedge}{\psi} = \begin{bmatrix} 0 & -\psi_z & \psi_y \\ \psi_z & 0 & -\psi_x \\ -\psi_y & \psi_x & 0 \end{bmatrix} \tag{14}$$

$\forall \mathbf{r}_0 \in \mathbb{R}^3$, thus, $\mathbf{r}_0$ can be eliminated. It can be concluded from (12) and (13) as follow:

$$\mathbf{M}(t) = \overset{\wedge}{\psi} \cdot \mathbf{R}^r(t). \tag{15}$$

$\overset{\wedge}{\psi}$ is obtained by the least square method as follows:

$$\overset{\wedge}{\psi} = (\mathbf{W}^T \cdot \mathbf{W})^{-1} \cdot \mathbf{W}^T \cdot \mathbf{M}(t) \tag{16}$$

where $\mathbf{W}$ can be express as

$$\mathbf{W} = \left\{ \begin{bmatrix} 0 & R_{3,1}^r & -R_{2,1}^r \\ -R_{3,1}^r & 0 & R_{1,1}^r \\ R_{2,1}^r & -R_{1,1}^r & 0 \end{bmatrix}, \begin{bmatrix} 0 & R_{3,2}^r & -R_{2,2}^r \\ -R_{3,2}^r & 0 & R_{1,2}^r \\ R_{2,2}^r & -R_{1,2}^r & 0 \end{bmatrix}, \right.$$
$$\left. \begin{bmatrix} 0 & R_{3,3}^r & -R_{2,3}^r \\ -R_{3,3}^r & 0 & R_{1,3}^r \\ R_{2,3}^r & -R_{1,3}^r & 0 \end{bmatrix} \right\} \tag{17}$$

$\overrightarrow{\mathbf{\Omega}}_{eff}(t)$ can be obtained by (3), the cross-range vector $\overrightarrow{\mathbf{f}}_d(t)$ of ISAR image can be expressed as

$$\overrightarrow{\mathbf{f}_d}(t) = \overrightarrow{\mathbf{\Omega}}_{eff}(t) \times \mathbf{L}(t). \tag{18}$$

ISAR imaging plane normal vector $\mathbf{Z}_i(t)$ is

$$\mathbf{Z}_i(t) = \mathbf{L}(t) \times \overrightarrow{\mathbf{f}_d}(t). \tag{19}$$

The direction vector of the spacecraft Main axis$(O_t Z_s)$ in the roll coordinate system at the starting time is

$$\boldsymbol{l_0} = [0, \sin\theta, \cos\theta]^{\mathrm{T}}. \tag{20}$$

For spin has no effect on the Main axis, the direction vector of the Main axis in the roll coordinate system is

$$\mathbf{r_l}(t) = \mathbf{R_{coni}}(t) \cdot \mathbf{R_{init}} \cdot \boldsymbol{l_0}. \tag{21}$$

The direction vector $\mathbf{MA}(t)$ of the spacecraft's Main axis in the imaging coordinate system can be expressed as

$$\mathbf{MA}(t) = \mathbf{C}_{p2j} \cdot \mathbf{r_l}(t) \tag{22}$$

where $\mathbf{C}_{p2j}$ can be express as

$$\mathbf{C}_{p2j} = \begin{bmatrix} \cos\gamma_{p2j} & \sin\gamma_{p2i} & 0 \\ -\sin\gamma_{p2j} & \cos\gamma_{p2j} & 0 \\ 0 & 0 & 1 \end{bmatrix} \begin{bmatrix} \cos\beta_{p2j} & 0 & -\sin\beta_{p2j} \\ 0 & 1 & 0 \\ \sin\beta_{p2j} & 0 & \sin\beta_{p2j} \end{bmatrix}$$
$$\begin{bmatrix} 1 & 0 & 0 \\ 0 & \cos\alpha_{p2j} & \sin\alpha_{p2j} \\ 0 & -\sin\alpha_{p2j} & \cos\alpha_{p2j} \end{bmatrix}. \tag{23}$$

IV. METHOD OF SPACECRAFT AXIAL ATTITUDE ESTIMATION

A. Axial Extraction of ISAR Image Based on Morphological Linear Structure Erosion

Hough or radon transform is often used to detect straight lines in ISAR images [25], [26]. There are many adverse factors such as angular flicker, cavity scattering, partial occlusion, and even image defocusing in ISAR images. There adverse factors will introduce a large number of local maxima to Hough or Radon transform and greatly reduce the accuracy of direction analysis. In this article, the erosion of morphological linear structural elements are proposed to analyze the global direction of ISAR image [27], [28].

Morphological erosion is defined as the structural element $\mathbf{B}(\varphi, \phi)$ to corrode the gray image $\mathbf{I}(s, t)$, where φ means angle, ϕ means length, (s, t) means the gray image coordinates. Morphological erosion is expressed as $\mathbf{I} \ominus \mathbf{B}$. The mathematical expression of morphological corrosion is as follows:

$$\mathbf{I} \ominus \mathbf{B} = \min\{\mathbf{I}(s + \varphi, t + \phi) - \mathbf{B}(\varphi, \phi)\} \tag{24}$$

where $(s + \varphi, t + \phi) \in D_f, (\varphi, \phi) \in D_b$, here D_f and D_b are the domains of $\mathbf{I}$ and $\mathbf{B}$, respectively.

In this article, the line segment is taken as the structural element, which is called the linear structural element. The linear structural element $\mathbf{B}(\varphi, \phi)$ with different angle ϕ and length φ can be used to corrode $\mathbf{I}$ of the image, respectively. When the direction of linear structural element is the same as that of image structure, the erosion amount of image is less than that of other directions. Therefore, by finding the maximum value of image volume ratio before and after erosion of linear structural elements with different angles, we can determine the overall structure direction of the image, namely

$$\phi = \underset{\phi}{\mathrm{argmax}} \left\{ \frac{\mathrm{sum}[\mathbf{I} \ominus \mathbf{B}(\varphi, \phi)]}{\mathrm{sum}(\mathbf{I})} \right\}. \tag{25}$$

The linear structure element length φ needs to be set according to the size of the spacecraft structure. Here, the axial estimation only considers the direction, and is independent of the spacecraft size and the center position of spacecraft in the ISAR image.

B. Attitude Estimation of Spacecraft in Orbit

(1) Attitude estimation of spacecraft Main axis.

In the imaging coordinate system, the projection $\mathrm{proj}_{\mathbf{x_i o_t y_i}}[\mathbf{MA}(t_j)]$ of the spacecraft's Main axis $\mathbf{MA}(t)$ on the imaging plane $\mathbf{X_i O_t Y_i}$ at $t_j (j = 1, 2, \ldots, n)$ time can be expressed as

$$\mathrm{proj}_{\mathbf{x_i o_t y_i}}[\mathbf{MA}(t_j)] = \mathbf{MA}(t_j) - \mathrm{proj}_{\mathbf{L}(t_j)}[\mathbf{MA}(t_j)]$$
$$= \mathbf{MA}(t_j) - \frac{\mathbf{MA}(t_j) \cdot \mathbf{L}(t_j)}{\|\mathbf{L}(t_j)\|} \cdot \mathbf{L}(t_j). \tag{26}$$

Among them, $\mathbf{L}(t_j)$ is the LOS vector at the time t_j, which can be calculated by (1). $\phi(t_j)$ represents axis direction of ISAR image at t_j time, and the normalized judgment function $f_{t_j}(\theta, \omega, \alpha_{p2j}, \beta_{p2j}, \gamma_{p2j})$ can be defined as follows:

$$f_{t_j}(\theta, \ldots, \gamma_{p2j}) = \mathrm{argz}\{\mathrm{proj}_{\mathbf{x_i o_t y_i}}[\mathbf{MA}(t_j)]\} - \phi(t_j). \tag{27}$$

Where the function argz represents the angle between $\mathrm{proj}_{\mathbf{x_i o_t y_i}}[\mathbf{MA}(t_j)]$ and $\mathbf{O_t X_i}$. In (27), there are five unknown parameters: $\theta, \omega, \alpha_{p2j}, \beta_{p2j}$, and γ_{p2j}. At least 5 ISAR images containing spacecraft's different attitude are needed to get an unique solution. It is difficult to directly solve the equation. Alternatively, the solution of abovementioned formula is transformed into a minimization problem as following:

$$\begin{cases} \mathrm{find}: X = (\theta, \omega, \alpha_{p2j}, \beta_{p2j}, \gamma_{p2j}) \\ \min: F(X) = \sum_{j=1}^n f_{t_j}^2(\theta, \omega, \alpha_{p2j}, \beta_{p2j}, \gamma_{p2j}) \\ s.t. \quad \theta \in [0, \pi], \omega \in [0, \infty), (\alpha_{p2j}, \beta_{p2j}, \gamma_{p2j}) \in [0, 2\pi]. \end{cases} \tag{28}$$

In this article, single point metamorphosis evolutionary programming (SPMEP) algorithm [29] is used to solve (28), which has some advantage and stability in solving high-dimensional multimode function problems. The basic steps are as follows.

Step 1: A population composed of n individuals is randomly generated, the initial number of iterations is $m = 1$. Each individual is represented by a real number pair (x_i, η_i), $\forall i \in \{1, 2, \ldots, n\}$, where $\boldsymbol{x_i} = (\theta, \omega, \alpha_{p2j}, \beta_{p2j}, \gamma_{p2j})$ is the target variable and η_i is the standard deviation of the normal distribution with the mean value of zero.

Step 2: The objective function $F(x_i)$ of each individual in the population is calculated.

Step 3: For each individual (x_i, η_i), a unique descendant (x'_i, η'_i) is generated by the following formula:

$$\begin{cases} \mathrm{x}'_i(k_i) = \mathrm{x}_i(k_i) + \eta_i N_i(0, 1) \\ \eta'_i(k_i) = \eta_i(k_i)\exp(-\varepsilon). \end{cases} \quad (29)$$

Where $x_i(k_i), x'_i(k_i), \eta_i(k_i), \eta'_i(k_i)$, respectively, represent the k_i components of vectors $x_i, x'_i, \eta_i, \eta'_i$ and are randomly selected numbers in the set $\{1, 2, \ldots, n\}$, and $N_i(0, 1)$ is standard normal distribution. The parameter ε is usually set to 1.01.

Step 4: The objective function $F(x_i')$ of each offspring (x'_i, η'_i) was calculated, and all the parent individual (x_i, η_i) and the child individual (x'_i, η'_i) were compared, and n individuals with high objective function value were selected to form the next generation population.

Step 5: If the maximum iteration or minimum error criterion is satisfied, break the current iteration and turn to Step 6; otherwise, $m = m + 1$ turn to Step 3.

Step 6: Choosing the best individual as the optimal solution of the algorithm, $\widetilde{\boldsymbol{x_i}} = (\widetilde{\theta}, \widetilde{\omega}, \widetilde{\alpha}_{p2j}, \widetilde{\beta}_{p2j}, \widetilde{\gamma}_{p2j})$.

(2) Estimation of spin period of axis symmetric spacecraft.

For an axis symmetric spacecraft similar to Tiangong-1, after the spacecraft's Main axis is estimated, the main body is removed from the ISAR image, so the solar array is left. Similarly, the axial extraction method of linear structure erosion is used, and the projection of the solar array on the imaging plane at t_j time is $\phi_f(t_j)$. It can define the normalized judgment function as follows:

$$f(t_j)(\Omega, L) = \mathrm{argz}\{\mathrm{proj}_{\mathbf{x_i o_t y_i}}[\mathbf{r}(t_j) + L \cdot \mathbf{MA}(t_j)]\} - \phi_f(t_j). \quad (30)$$

Where $\mathbf{r}(t_j)$ is the position vector of $\mathbf{r}(t)$ at time t_j, L is the length from the centroid O_t to the intersection point C_t of the sailboard and the Main axis. The spin angular velocity Ω can be similarly solved by the same method as the attitude estimation of Main axis.

C. Algorithm Flow Chart

According to the abovementioned analysis, the flowchart of attitude estimation algorithm of spacecraft in orbit is shown in the Fig. 6. In this method, the following necessary conditions need to be satisfied.

1) ISAR image sequence have been cross-range scaled; The clarity of each ISAR image used needs to ensure that the axis can be extracted.
2) The orbit position and velocity of the spacecraft, location, and imaging parameters of radar are all accurate known. The influence of orbit perturbation and other factors is included in the orbit calculation model, such as simplified general perturbations 4 model. It is not considered that the
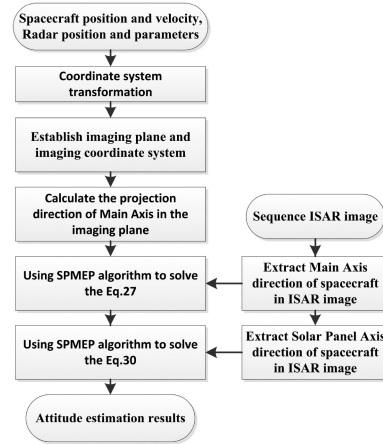

Fig. 6. Flowchart of the proposed attitude estimation algorithm.

influence of other nonorbit model errors for Axial attitude estimation.
3) In the time of ISAR imaging sequence, the roll period, roll axis, and spin period of the spacecraft remain unchanged. The spacecraft is a rigid body without component micromotion [30].

V. EXPERIMENTS

In this part, based on simulation data and measurement data, four experiments are carried out to verify the feasibility and effectiveness of our method.

Part A: The purpose is to verify the accuracy of imaging plane selection for rolling attitude spacecraft. First, the radar echo of point target is simulated, and the sequence ISAR image is obtained by RD algorithm, and the scattering point position of sequence ISAR image is extracted. According to the conclusion derived from Section III, the position of the imaging plane in J2000.0 inertial coordinate system is calculated, and then the 3-D coordinates of the target are projected onto the imaging plane to obtain the sequence "projection image". Finally, by comparing the position coordinates of the scattering points extracted from the sequence ISAR image and the sequence "projection image" points, the correctness of the derivation of the imaging plane is proved, and the problem of selecting the time of the imaging plane is also analyzed.

Part B: Based on the ISAR image sequence of international cargo ship published by FGAN Laboratory of TIRA radar, where the spacecraft has "cavity scattering," "angular glint," "high sidelobe," "image defocus," and "no rectangular feature" in different attitude angles. The robustness of ISAR axial extraction based on morphological linear structure erosion method is verified.

Part C: The rolling attitude of Tiangong-1 is estiamted using simulation ISAR image sequence, which verifies the accuracy of this method. Under the environment of windows 10 personal edition system, 3dmax modeling and physical optics method are used to simulate echo data. According to the real two-line element (TLE) data, the measurement parameters of orbit and radar visible period are calculated, the flight state model in orbit is established. The radar echo of Tiangong-1 is generated by
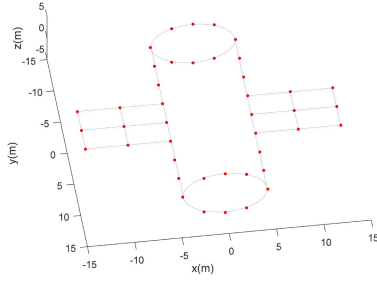
Fig. 7. Three-dimensional distribution of points.

TABLE II
MAIN PARAMETERS OF SPACECRAFT ORBIT

Parameter	Quantity
Altitude	$380km$
Inclination	42.7824°
Period	$92.219min$

TABLE III
MAIN PARAMETERS OF ISAR IMAGING RADAR FOR POINTS MODEL

Parameter	Quantity
Center of frequncy	$9GHz$
Bandwidth	$1GHz$
Pulse repetition interval	$0.05s$
Pulse width	$5\mu s$
Coherent processing interval	$12.8s$
Number of pulse	256
Longitude	66.17°
Latitude	25.78°
Height	$0m$

simulation, and the ISAR image sequence is generated by RD algorithm. The attitude of Tiangong-1 is estimated by tracking the measured parameters and the corresponding ISAR image sequence. For attitude stabilization spacecraft, the attitude has been given in [6], [14], and [31]. The experiment only estimates the parameters of Tiangong-1 in the case of attitude rolling.

Part D: ISAR image sequence of Tiangong-1 published by FGAN laboratory were used to analyze the rolling state of Tiangong-1 before the re-entry. This experiment is to verify the practicability of this method.

A. Analysis Imaging Plane for Rolling Attitude Spacecraft

In the experiment, 42 points are used to simulate a 3-D spacecraft model, which consists of a cylindrical body and two solar panels. The 3-D distribution of model is shown in Fig. 7. The spacecraft adopts a near circular orbit with a simulation time of 500 s. The main parameters of orbit are shown in Table II. The radar parameters are shown in the Table III. Considering the earth rotation, the trajectories of radar and spacecraft in the simulation time are shown in Fig. 8. We analyzed three kinds of attitude of spacecraft: Inertial stable, triaxial stable, and roll. Three-axis stability mode is that the three vertical axes of the satellite must be controlled at the same time to prevent the rotation and swing of any axis from exceeding the specified value, and usually one axis points to the earth center. Inertial
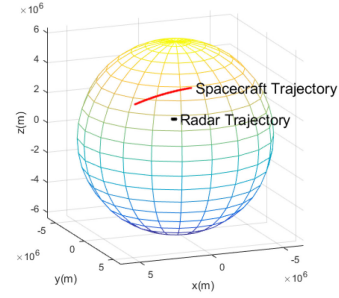

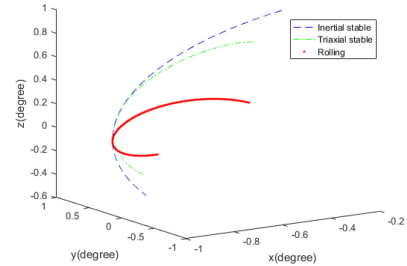Fig. 8. Trajectories of radar and spacecraft.

Fig. 9. Normal direction of the imaging plane for the three attitudes.

stability mode method keeps the axes in the object-fixed coordinate system parallel to fixed vectors in the inertial system. The roll attitude parameters are $\theta = 30^\circ$, $\omega = 0.25^\circ$/s, $\Omega = 0.02^\circ$/s. In the whole simulation time, the normal direction of the imaging plane for the three attitudes is shown in Fig. 9.

RD algorithm is used to image the simulated production radar echo, and ISAR image results are shown in the Fig. 10(a). Clean algorithm [32] is used to roughly extract the scattering points of ISAR image, which can preliminarily remove the interference of side lobe. Then, Ostu algorithm [33] is used to precisely extract the scattering points in the rough extracted scattering point area. The result of scattering point extraction is shown in the Fig. 10(b). The projection image is defined as the orthographic projection of the imaging plane of the 3-D spacecraft model at time t_p. We define the beginning time of CPI as t_0, the middle time of CPI as t_m, the end time of CPI as t_e. It is shown that the projected image at t_0, t_m, and t_e in the Fig. 10(c).

In Fig. 10(b), the coordinate of the scattering point corresponding to the nth point on the 3-D spacecraft model is defined as $A_n = (x_n, y_n)$, $n \in [1, 2, \ldots, 42]$. In Fig. 10(c), at the imaging time t_p, the projection image coordinates of the nth point on the 3-D model is defined as $B_n^m = (a_n^m, b_n^m)$, m is the index of pulse in CPI, $m \in [0, 1, \ldots, 255]$, $t_p = t_0 + m * \text{PRI}$. The similarity function between time Fig. 10(b) and time Fig. 10(c) is defined as (31). The similarity curve of the whole CPI is shown in the Fig. 10(d). From the minimum point of similarity curve $m = 127$, it can be concluded that the projection image is closest to ISAR at t_m time. So the following projection images in this article refer to $t_p = t_m$

$$\text{Sim}(m) = \frac{1}{42} \sum_{n=1}^{42} |A_n - B_n^m|. \tag{31}$$
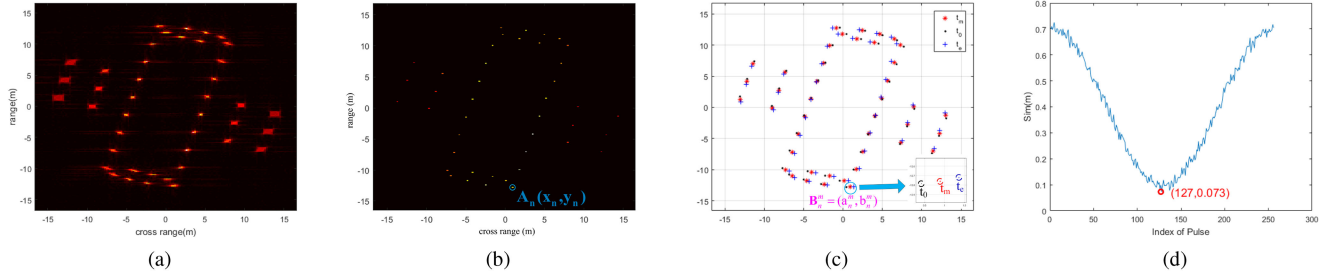
Fig. 10. ISAR image and projection image. (a) ISAR image. (b) Scattering point extraction from ISAR image. (c) Projection images at different CPI time. (d) Similarity curve of the whole CPI.
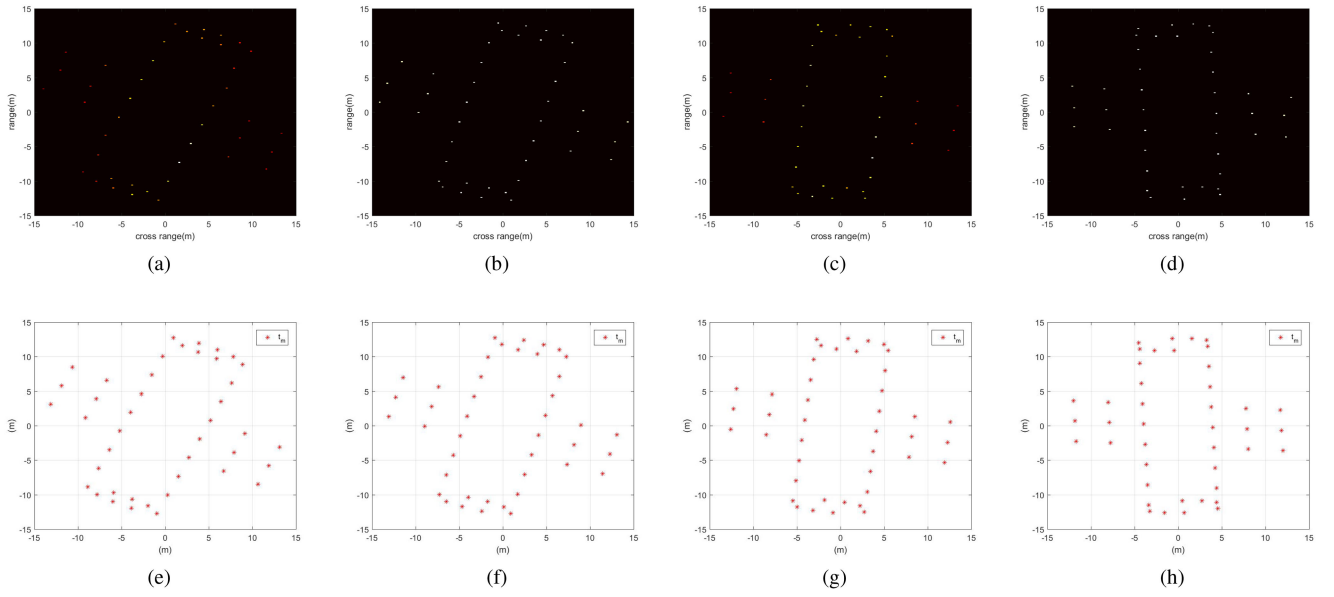

Fig. 11. Sequence of ISAR scattering images and projection images. (a), (b), (c), (d), are the ISAR scattering point extraction results, (e), (f), (g), (h) are the sequence projection images.
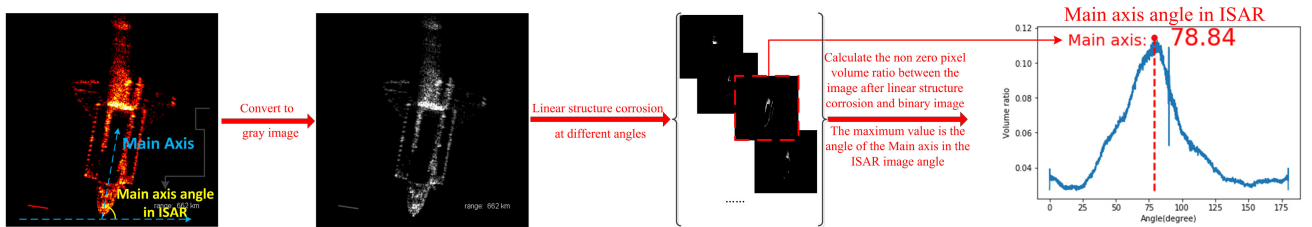

Fig. 12. Main axis estimation process by morphological linear structure erosion.

In Fig. 11, (a)–(d) is the ISAR scattering point extraction results, (e)–(h) is the sequence projection images. According to 31, Sim between (a) and (e) is 0.191 m, that between (b) and (f) is 0.073 m, that between (c) and (g) is 0.098 m and that between (d) and (h) is 0.176 m. From the comparison between the sequence projection images and ISAR scattering point extraction results, it can be concluded that the derivation of the imaging plane position in Section III-B is correct. The position deviation is mainly caused by the extraction error of ISAR scattering points.

B. Axial Extraction of Measured ISAR Image

As shown in Fig. 12, Main axis angle in ISAR is estimated by morphological linear structure erosion. The image width is W, the linear erosion structure φ is set to $W/10$, and the sampling accuracy of the angle ϕ is $0.01°$. Two adjacent measured ISAR image of Cargo is shown in Fig. 13(a) and (b). Scale-invariant feature transform [34] features are extracted in Fig. 13(a1) and (b1). There are angular glint and cavity scattering phenomenon in these ISAR images, where scattering points change
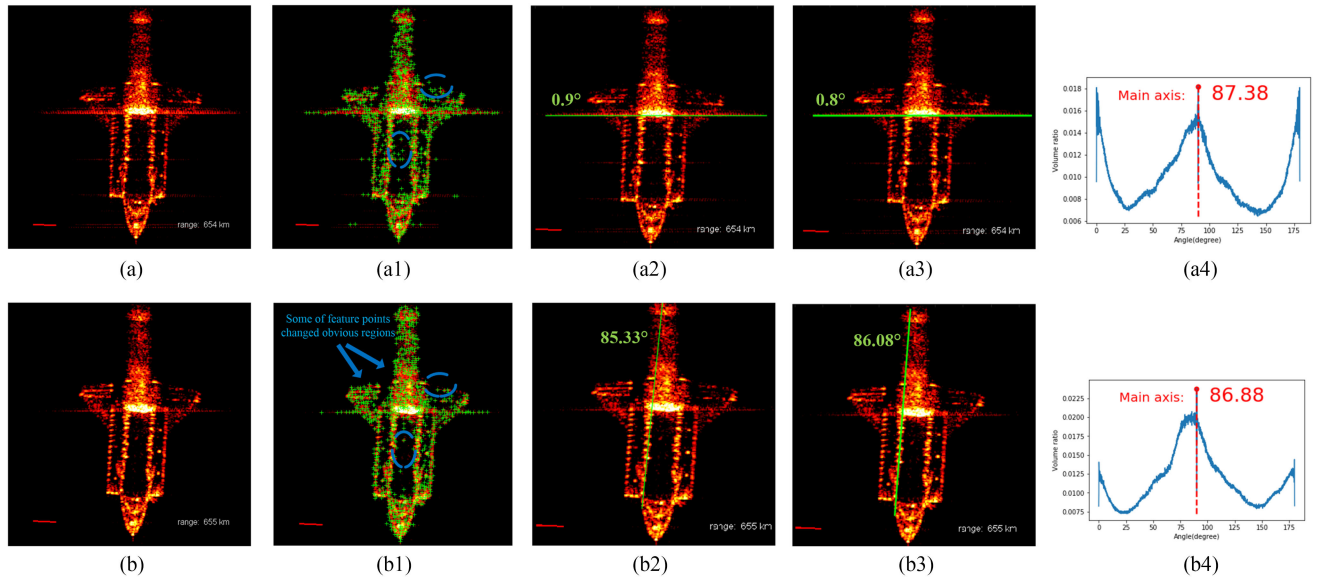
Fig. 13.   Main axis estimation process by morphological linear structure erosion.
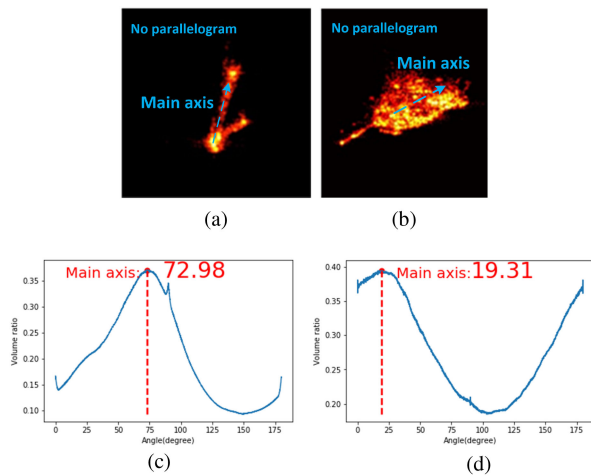

Fig. 14.   Main axis estimation of measured ISAR images.

TABLE IV
MAIN PARAMETERS OF ISAR IMAGING RADAR

Parameter	Quantity
$Center\ of\ freqency$	$16.7GHz$
$Bandwidth$	$2GHz$
$Pulse\ repetition\ frequency$	$100Hz$
$Range\ resolution$	$0.075m$
$Cross-range\ resolution$	$0.075m$
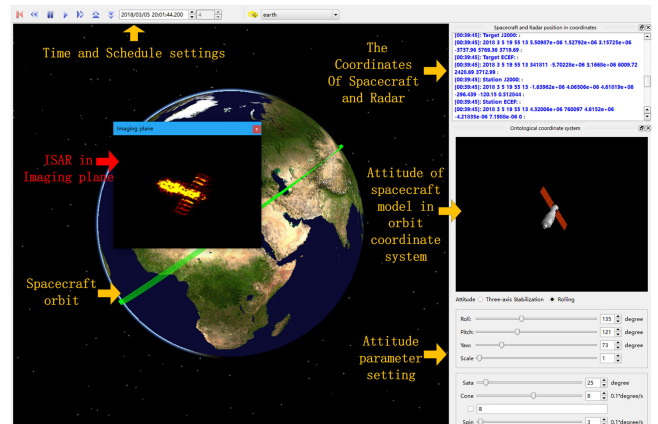
Fig. 15.   Simulation software for attitude estimation of spacecraft in orbit.

significantly in adjacent images. The core of "factorization method" is feature point extraction and matching, so this method could be failed. In Fig. 13(a2) and (a3), Hough transform and Radon transform can not detect the correct Main axis direction due to the high sidelobe formed by strong scattering points.

ISAR images and Main axis extraction results of other spacecrafts are shown in Fig. 14. The core of "the parallelogram feature" method is to detect parallel lines. In Fig. 14(a) and (b), it is difficult to find rectangular feature in ISAR images, so this method could be failed. In all those figures abovementioned, the method proposed by this article can still estimate the Main axis angle in ISAR images. The results are shown in Fig. 13(a4) and (b4) and Fig. 14(c) and (d). So compared with previous methods, our proposed method is more robust.

C. Attitude Estimation of Tiangong-1 Using Simulated Data

In this Part, the TIRA radar in Germany is taken for reference, which is located in Wachtberg area and affiliated to FGAN Lab in Germany. The main parameters of the ISAR imaging radar are listed in Table IV. Our simulation system interface is shown in Fig. 15. In Table V, TLE epoch uses the universal time coordinated (UTC), "observation duration" means the visible time of the radar to the spacecraft, such as "558.61 s" means

TABLE V
ATTITUDE ESTIMATION RESULTS FOR EVERY OBSERVATION TIME USING SIMULATION ISAR IMAGES

| Observation Time	TLE epoch (UTC)	Observation duration	Estimation Error of Yaw α_{p2j}	Estimation Error of Pitch β_{p2j}	Estimation Error of Roll γ_{p2j}	Estimation Error of rotation angle θ	True value of cone rotation Speed ω	Estimation of cone rotation Speed ω	True value of spin rotation Speed Ω	Estimation of spin rotation Speed Ω
Time 1	2018-03-05 10:12:55.944	558.61s	2.11°	2.71°	3.02°	5.93°	0.8°/s	0.65°/s	0.3°/s	0.32°/s
Time 2	2018-03-10 11:43:53.155	515.59s	3.90°	5.27°	1.67°	5.59°	0.8°/s	0.89°/s	0.3°/s	0.27°/s
Time 3	2018-03-16 14:51:47.045	256.57s	5.34°	4.17°	4.15°	6.48°	0.8°/s	1.09°/s	0.3°/s	0.22°/s
Time 4	2018-03-22 13:17:30.485	403.44s	4.82°	1.28°	4.30°	6.15°	0.8°/s	0.67°/s	0.3°/s	0.34°/s
Time 5	2018-03-27 14:51:47.045	341.55s	3.62°	2.43°	1.66°	1.13°	0.8°/s	0.61°/s	0.3°/s	0.37°/s
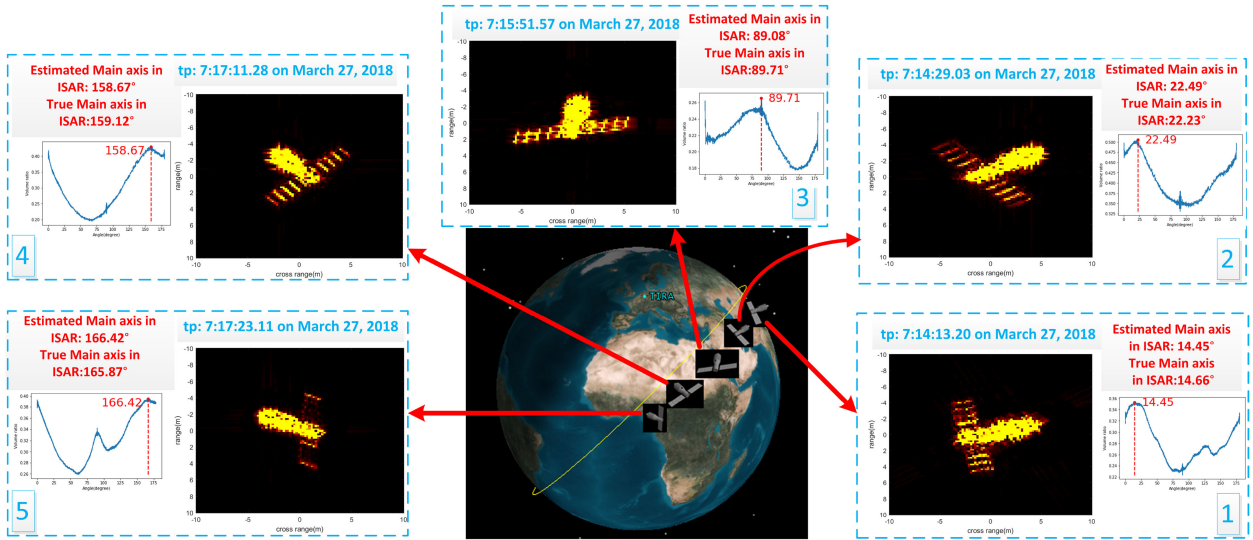
Fig. 16. Simulation of TIRA radar imaging Tiangong-1.

from "2018-03-05 19:55:01.24" to "2018-03-05 20:04:19.85" at "Time 1".

During the observation simulation, Tiangong-1 rolled in orbit. The linear erosion structure φ is set as 5 pixel, and the sampling accuracy of angle ϕ is $0.01°$. Simulated ISAR images of Tiangong-1 are shown in Fig. 16. The accuracy of attitude parameter estimation depends on the diversity of ISAR imaging angles. To solve the minimization problem in (26), the population number n is 100 and the maximum iteration number is 200. As shown in Table V, the estimation results of attitude parameters are obtained from six ISAR images, the proposed algorithm ensures $5°$ level estimation precision.

When the observation angle span of imaging is large enough and the diversity is sufficient enough, the error of the estimation results is obviously decreased. At "Time 1" in Table V, the relationship between the number of ISAR images and absolute error are shown in Fig. 17. According to the curve, when the number of ISAR images is more than 30, the error is basically stable. In general, the attitude estimation errors of axis are controlled about $2°$ while the estimation result of the rotation speed is close to the true value.

D. In Orbit Attitude Estimation of Tiangong-1 Using Measured Data

FGAN laboratory published the sequence ISAR imaging results of Tiangong-1 at an orbit height of 270 km [22]. The orbit
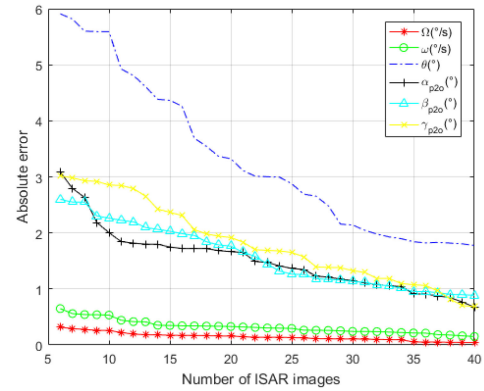

Fig. 17. Relationship between the number of ISAR images and absolute error. Absolute error=|True − Estimation|.

was calculated by real TLE data published at UTC 17:00 on February 23, 2018. From the ISAR image sequence, it can be confirmed that Tiangong-1 has a complete structure without breakup. According to the orbit parameters at that time, the attitude estimation method in this article is used to estimate Rolling parameters before re-entry. The measured ISAR results are shown in Fig. 18. The estimated results are shown in Table VI.

According to the post analysis results, Tiangong-1 re-entered at about 0:15:00 on April 2, 2018 UTC. According
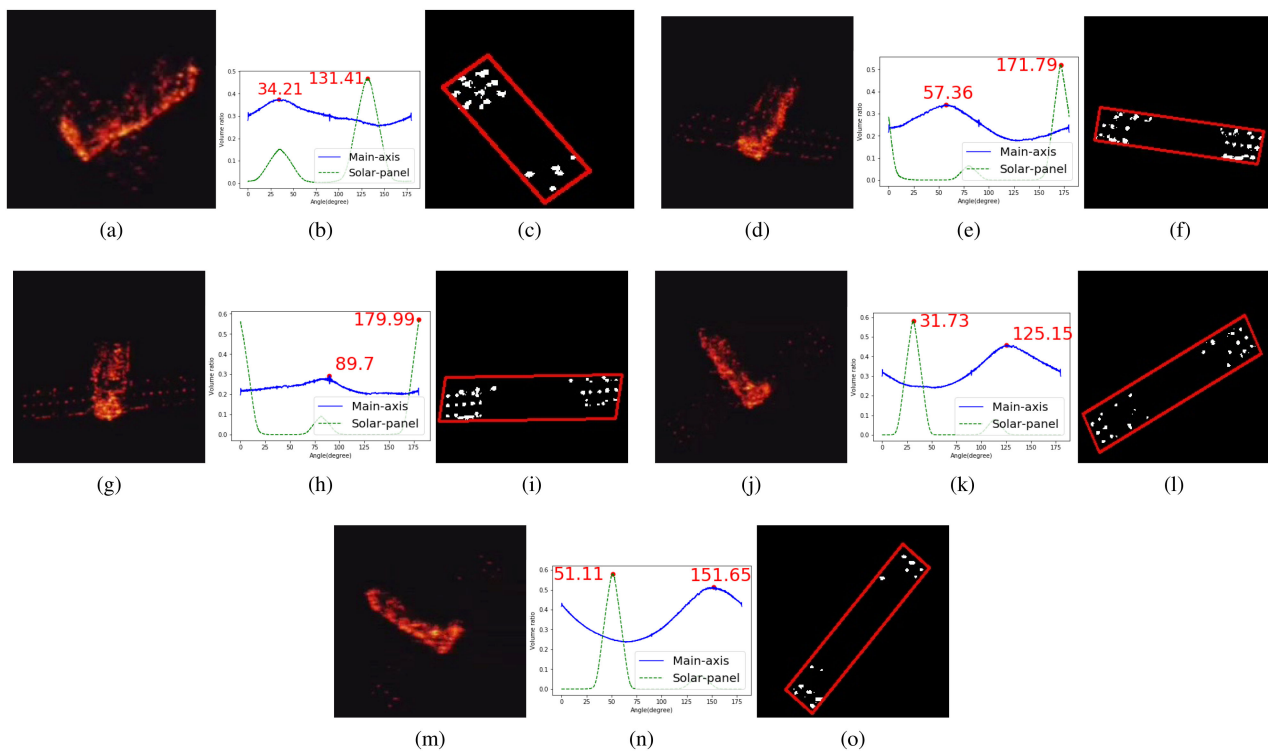
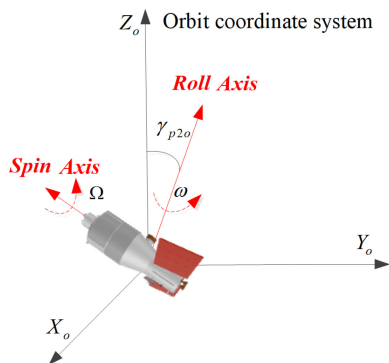Fig. 18. Measurement of ISAR image of Tiangong-1 by TIRA radar.

Fig. 19. Schematic diagram of Tiangong-1 rolling before re-entry.

Fig. 20. Relationship between every LOS in a single ISAR imaging time.

TABLE VI
ATTITUDE ESTIMATION RESULTS OF TIANGONG-1 MEASURED DATA

	θ	ω	Ω	α_{p2j}	β_{p2j}	γ_{p2j}
$Estimate$	$93.47°$	$1.18°/s$	$0.12°/s$	$20.67°$	$52.05°$	$41.72°$

to the measured ISAR image of TIRA radar, it can be estimated that Tiangong-1 was in the state of slow roll at that time, and the roll axis was about perpendicular to the solar panel, and Fig. 19 is the schematic diagram of Tiangong-1 roll. Our result is basically consistent with FGAN laboratory result [22].

VI. CONCLUSION

In this article, a method is proposed to estimate the attitude of spacecraft based on ISAR image sequence in orbit. First, the position of the ISAR imaging plane is derived in various orbit attitudes. Then, the direction of the Main axis in the ISAR image sequence is estimated. So the attitude estimation equation can be established by the relationship between the spatial coordinate systems. Finally, SPMEP algorithm is used to optimize the solution results. Compared with the existing methods, the proposed method neither need establish a simulation database, nor does it need the spacecraft to have some special structure. It only needs the axial linear feature in ISAR image sequence.

In the actual estimation of attitude parameters, the influence of the position and velocity error of the target in orbit, the
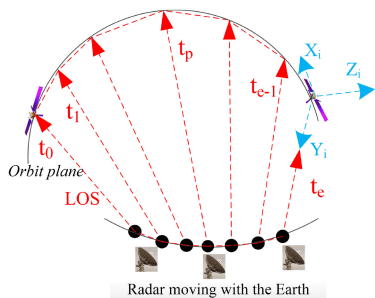
ISAR image scaling error and the truncation error of coordinate transformation should also be considered. In practical application, long-time observation can also be used to further improve the estimation accuracy. Other optimization algorithms may be better than SPMEP algorithm to further reduce the estimation error. This method is not only suitable for Tiangong-1, but also for other spacecrafts. In the further work, the influence of orbit parameters error on attitude estimation will be considered.

APPENDIX A
DETAILED DEFINITIONS OF THE COORDINATE SYSTEMS

(1) J2000.0 inertial coordinate system $O - X_j Y_j Z_j$.

The coordinate origin is the earth's centroid O, the basic plane is the 2000.0 earth's equatorial plane, and the axis X_j points from the earth's centroid O to the 2000.0 equinox in the basic plane. The axis Z_j is the normal direction of the basic plane, pointing to the north pole, and the axis Y_j, X_j, Z_j form a right-hand system.

(2) Orbit coordinate system $O_t - X_o Y_o Z_o$.

The coordinate origin is O_t. The axis Z_o points from the centroid of the spacecraft to the center of Earth, the axis Y_o points to the negative normal direction of the orbital plane, the axis X_o is perpendicular to the axis in the orbital plane and points to the direction of motion of the spacecraft, and the axis X_o, Y_o, Z_o forms a right-handed system.

(3) Transformation of spacecraft from J2000.0 coordinate system to orbit coordinate system. In J2000.0 inertial coordinate system, the position vector and velocity vector of the spacecraft at the imaging time t are r, $\dot{r}$. It can be obtained by precise orbit determination of radar measurement data or extrapolation of orbital elements

$$C_{j2o}(3, \text{i}) = \frac{r}{|r|} \tag{32}$$

$$C_{j2o}(2, \text{i}) = -\frac{r \times \dot{r}}{|r \times \dot{r}|} \tag{33}$$

$$C_{j2o}(1, \text{i}) = C_{j2o}(2, \text{i}) \times C_{j2o}(3, \text{i}) \tag{34}$$

where $i = 1, 2, 3$ corresponds to three components of each row vector in the transformation matrix C_{j2o}.

APPENDIX B
SELECTION OF EQUIVALENT IMAGING TIME t_p

According to the RD imaging algorithm [23], cross-range resolution requires a certain amount of rotation angle accumulation, i.e., imaging requires a certain amount of frame accumulation. When imaging spacecraft, the maximum elevation angle of radar tracking segment is generally less than $90°$, so the radar is generally not in the target orbit plane, i.e., the LOS of each time is not coplanar. If the time of angle accumulation is long, the change of radar position in inertial system caused by earth rotation should be considered. As shown in Fig. 20, the Radar LOS of $t_0, \ldots, t_p, \ldots, t_e$ is usually not in the same plane.

The imaging plane can be defined as the plane determined by the negative direction of radar's Line of sight as LOS_{t_p} and the equivalent observation angular velocity $\overrightarrow{\Omega}_{eff}$ of spacecraft

motion at t_p time. In general, the zero points of range and cross-range coordinates of ISAR image are in the center of the image, so the reference frame of range alignment should select the zero time frame of Doppler frequency shift, so t_p is selected as the middle time of CPI, i.e., $t_p = \frac{t_o + t_e}{2}$. This conclusion can be proved by Fig. 10 of the Experiment Part A.

REFERENCES

[1] N. Koshkin, E. Korobeynikova, L. Shakun, S. Strakhova, and Z. H. Tang, "Remote sensing of the EnviSat and Cbers-2B satellites rotation around the centre of mass by photometry," *Adv. Space Res.*, vol. 58, no. 3, pp. 358–371, 2016.

[2] L. Carozza and A. Bevilacqua, "Error analysis of satellite attitude determination using a vision-based approach," *ISPRS J. Photogrammetry Remote Sens.*, vol. 83, pp. 19–29, 2013.

[3] J. Rosebrock, "Absolute attitude from monostatic radar measurements of rotating objects," *IEEE Trans. Geosci. Remote Sens.*, vol. 49, no. 10, pp. 3737–3744, Oct. 2011.

[4] K. Suwa, T. Wakayama, and M. Iwamoto, "Three-dimensional target geometry and target motion estimation method using multistatic ISAR movies and its performance," *IEEE Trans. Geosci. Remote Sens.*, vol. 49, no. 6, pp. 2361–2373, Jun. 2011.

[5] J. T. Mayhan, M. L. Burrows, K. M. Cuomo, and J. E. Piou, "High resolution 3D "snapshot" ISAR imaging and feature extraction," *IEEE Trans. Aerosp. Electron. Syst.*, vol. 37, no. 2, pp. 630–642, Apr. 2001.

[6] J. Chen, T. Fu, D. Chen, and M. Gao, "Observation angle and plane characterisation for ISAR imaging of LEO space objects," *Adv. Space Res.*, vol. 58, no. 1, pp. 30–44, 2016.

[7] M. Ferrara, G. Arnold, and M. Stuff, "Shape and motion reconstruction from 3D-to-1D orthographically projected data via object-image relations," *IEEE Trans. Pattern Anal. Mach. Intell.*, vol. 31, no. 10, pp. 1906–1912, Oct. 2009.

[8] F. Wang, F. Xu, and Y. Jin, "3-D information of a space target retrieved from a sequence of high-resolution 2-D ISAR images," in *Proc. IEEE Int. Geosci. Remote Sens. Symp.*, 2016, pp. 5000–5002.

[9] R. Perrier, E. Arnaud, P. Sturm, and M. Ortner, "Satellite image registration for attitude estimation with a constrained polynomial model," in *Proc. IEEE Int. Conf. Image Process.*, 2010, pp. 925–928.

[10] F. Wang, T. F. Eibert, and Y. Jin, "Simulation of ISAR imaging for a space target and reconstruction under sparse sampling via compressed sensing," *IEEE Trans. Geosci. Remote Sens.*, vol. 53, no. 6, pp. 3432–3441, Jun. 2015.

[11] L. Liu, F. Zhou, X. Bai, J. Paisley, and H. Ji, "A modified EM algorithm for ISAR scatterer trajectory matrix completion," *IEEE Trans. Geosci. Remote Sens.*, vol. 56, no. 7, pp. 3953–3962, Jul. 2018.

[12] X. Yang, G. Wen, J. Zhong, B. Hui, and C. Ma, "A 3-D electromagnetic-model-based algorithm for absolute attitude measurement using wideband radar," *IEEE Geosci. Remote Sens. Lett.*, vol. 12, no. 9, pp. 1878–1882, Sep. 2015.

[13] S. Lemmens, H. Krag, J. Rosebrock, and I. Carnelli, "Radar mappings for attitude analysis of objects in orbit," in *Proc. Eur. Conf. Space Debris*, 2013, pp. 20–24.

[14] Y. Zhou, L. Zhang, Y. Cao, and Z. Wu, "Attitude estimation and geometry reconstruction of satellite targets based on ISAR image sequence interpretation," *IEEE Trans. Aerosp. Electron. Syst.*, vol. 55, no. 4, pp. 1698–1711, Aug. 2019.

[15] Y. Zhou, L. Zhang, and Y. Cao, "Dynamic estimation of spin spacecraft based on multiple-station ISAR images," *IEEE Trans. Aerosp. Electron. Syst.*, vol. 58, no. 4, pp. 2977–2989, Apr. 2020.

[16] L. Liu, F. Zhou, X. Bai, M. Tao, and Z. Zhang, "Joint cross-range scaling and 3D geometry reconstruction of ISAR targets based on factorization method," *IEEE Trans. Image Process.*, vol. 25, no. 4, pp. 1740–1750, Apr. 2016.

[17] H. Chen, J. Yang, and C. Ye, "Target rotation estimation for inverse synthetic aperture radar with sparse aperture and larger rotation angle," *Chin. J. Radar Sci.*, vol. 34, no. 1, pp. 70–75, 2019.

[18] Y. Liu, X. Li, S. Zhang, and G. Bi, "Fast ISAR cross-range scaling using modified newton method," *IEEE Trans. Aerosp. Electron. Syst.*, vol. 54, no. 3, pp. 1355–1367, Jun. 2018.

[19] D.-M. S. Sommer, J. Rosebrock, and L. Leushacke, "Temporal analysis of Envisat's rotational motion," in *Proc. Eur. Conf. Space Debris*, 2017.

[20] J.-N. Pittet and J. Silha, "Spin motion determination of the Envisat satellite through laser ranging measurements from a single pass measured by a single station," *Adv. Space Res.*, vol. 61, no. 4, pp. 1121–1131, 2018.

[21] C. Song, H.-Y. Lin, and C.-Y. Zhao, "Analysis of Envisat's rotation state using epoch method," *Adv. Space Res.*, vol. 66, no. 11, pp. 2681–2688, 2020.

[22] F. Lab, *Forscher Des Fraunhofer FHR Begleiten Wiedereintritt Der Chinesischen Raumstation Tiangong-1*. Mar. 2018. [Online]. Available: Available: https://www.fhr.fraunhofer.de/tiangong-bilder

[23] C. Chen and H. C. Andrews, "Target-motion-induced radar imaging," *IEEE Trans. Aerosp. Electron. Syst.*, vol. AES- 16, no. 1, pp. 2–14, Jan. 1980.

[24] V. C. Chen, *The Micro-Doppler Effect in Radar [M]*. Norwood, MA, USA: Artech House, 2011.

[25] P. Mukhopadhyay and B. B. Chaudhuri, "A survey of hough transform," *Pattern Recognit.*, vol. 48, no. 3, pp. 993–1010, 2015.

[26] P. Toft, "The radon transform theory and implemention," Ph.D. dissertation, Techn. Univ., Kongens Lyngby, Denmark, 1996.

[27] C.-C. Han and K.-C. Fan, "A greedy and branch and bound searching algorithm for finding the optimal morphological erosion filter on binary images," *IEEE Signal Process. Lett.*, vol. 1, no. 2, pp. 41–44, Feb. 1994.

[28] M. Abhayadev and T. Santha, "Object boundary identification using enhanced high pass frequency filtering algorithm and morphological erosion structuring element," *Procedia Comput. Sci.*, vol. 76, no. 147, pp. 158–164, 2019.

[29] M. Ji, H. Tang, and J. Guo, "A single-point mutation evolutionary programming," *Inf. Process. Lett.*, vol. 90, no. 6, pp. 293–299, 2004.

[30] Y. Liu, D. Zhu, X. Li, and Z. Zhuang, "Micromotion characteristic acquisition based on wideband radar phase," *IEEE Trans. Geosci. Remote Sens.*, vol. 52, no. 6, pp. 3650–3657, Jun. 2014.

[31] H. Chao-Ying, Y. Hong-Cheng, W. Xiao, X. Xiao-Yu, and M. Liang, "Attitude estimation method of space targets by 3D reconstruction of principal axis from ISAR image," *Procedia Comput. Sci.*, vol. 147, pp. 158–164, 2019.

[32] B. D. Steinberg and J. Tsao, "Reduction of sidelobe and speckle artifacts in microwave imaging: The clean technique," *IEEE Trans. Antennas Propag.*, vol. 36, no. 4, pp. 543–556, Apr. 1988.

[33] N. Otsu, "A threshold selection method from gray-level histograms," *IEEE Trans Syst., Man, Cybern.*, vol. 9, no. 1, pp. 62–69, Jan. 1979.

[34] D. G. Lowe, "Distinctive image features from scale-invariant keypoints," *Int. J. Comput. Vis.*, vol. 60, no. 2, pp. 91–110, 2004.

Peng Kou was born in Xi'an, China, in 1981. He received the B.S. degree in communication engineering in 2010 from the National University of Defense Technology, Changsha, China where he is currently working toward the Ph.D. degree in signal and information processing.

After working as a Senior Engineer with Xi'an Satellite Control Center for eight years. His current research interests include ISAR imaging and image interpretation.

Yongxiang Liu received the B.S. in communication engineering and Ph.D. degrees in information and communication engineering from the National University of Defense Technology (NUDT), Changsha, China, in 1999 and 2004, respectively.

He has been with NUDT Since 2004 and is currently a Professor with the College of Electronic Science and Technology. He was with Imperial College London as an academic visitor in 2008. His research interests include radar target recognition, time-frequency analysis, and micromotions.

Weijun Zhong was born in Zhejiang, China, in 1982. He received the M.Eng. and Ph.D. degrees in electronic engineering from Air Force Engineering University, Xi'an China, in 2009 and 2012, respectively.

From 2012 to 2019, his research focuses on the ISAR imaging, attitude inversion, and automatic target recognition.
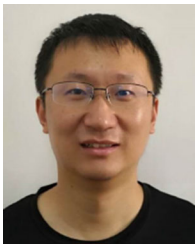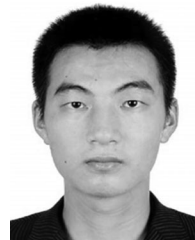
Biao Tian was born in Nanchong, China, in 1988. He received the B.S. and Ph.D. degrees in communication engineering from the National University of Defense Technology, Changsha, China, in 2011 and 2016, respectively.

He is currently an Associate Research Fellow with the National University of Defense Technology. His current research interests include radar signal processing and imaging.

Wenzhen Wu was born in Zaozhuang, China, in 1992. He received the B.S. degree in information engineering from Zhejiang University, Hangzhou, China, in 2014, and the M.S. degree in electronic science and technology from the National University of Defense Technology, Changsha, China, in 2016. He is currently working toward the Ph.D. degree in signal and information processing with the National Key Lab of Science and Technology on ATR, National University of Defense Technology.

His research interests include inverse synthetic aperture radar imaging, three-dimensional interferometric imaging, and automatic target recognition.

Chi Zhang received the B.S. degree in information engineering from Shanghai Jiao Tong University, Shanghai, China, in 2017. He is currently working toward the Ph.D. degree in information and communication engineering with National University of Defense Technology, Changsha, China.

His research interests include compressive sensing, Bayesian inference, machine learning and their applications in radar signal processing.